# Numerical Simulation of Local Calcium Movements During L-Type Calcium Channel Gating in the Cardiac Diad

C. Soeller and M. B. Cannell
Department of Pharmacology and Clinical Pharmacology, St. George's Hospital Medical School, London SW17 0RE, England

ABSTRACT Computer simulation was used to investigate the calcium levels after sarcolemmal calcium influx through L-type calcium channels (DHPRs) into the narrow diadic space of cardiac muscle. The effect of various cytosolic and membrane-bound buffers, diad geometry, DHPR properties (open time and current), and surface charge were examined. The simulations showed that phospholipid binding sites on the sarcolemmal membrane are the major buffer affecting free calcium ($[Ca^{2+}]$) levels in the diad. The inclusion of surface charge effects calculated from Gouy-Chapman theory resulted in a marked decrease in $[Ca^{2+}]$ levels at all times and a faster decay of $[Ca^{2+}]$ after termination of DHPR influx. For a DHPR current of 200 fA, $[Ca^{2+}]$ at the center of the diad reached peak levels of ~73 $\mu$M. In larger diads ($\geq$400 nm diameter), $[Ca^{2+}]$ decayed more slowly than in smaller diads (100–200 nm diameter), although peak $[Ca^{2+}]$ levels reached during typical DHPR open times were similar. For a wide range of DHPR single-channel current magnitudes ($I_{Ca}$ = 25–200 fA), $[Ca^{2+}]$ levels in the diad were approximately proportional to $I_{Ca}$. The decrease in calculated $[Ca^{2+}]$ levels due to the effects of surface charge can be interpreted as resulting from an effective "volume expansion" of the diad space. Furthermore, the layer of increased $[Ca^{2+}]$ close to the sarcolemmal membrane can act as a fast buffer.

## INTRODUCTION

Cardiac contraction occurs when the free intracellular calcium concentration ($[Ca^{2+}]$) increases from ~100 nM to ~1–2 $\mu$M. This increase in $[Ca^{2+}]$ is mainly due to calcium release from intracellular stores (the sarcoplasmic reticulum, SR), which can be triggered by a smaller calcium influx across the surface membrane via L-type calcium channels (DHPRs) when the cell depolarizes (see Bers, 1991, for a review). The process by which a small calcium trigger can cause a much larger calcium release is known as "calcium-induced calcium release" (CICR) (Fabiato, 1983), and this mechanism resides in the calcium-dependent gating behavior of SR calcium release channels.

There is now compelling evidence for the idea that cardiac E-C coupling is regulated by local calcium changes rather than the average cytoplasmic $[Ca^{2+}]$ level (e.g., López-López et al., 1994, 1995; Cannell et al., 1994, 1995). Thus to fully understand how cardiac E-C coupling is regulated, it will be important to understand the local changes in calcium produced by L-type calcium channel activity. Recently a numerical study has suggested that local $[Ca^{2+}]$ concentrations of more than 1 mM can be achieved (Langer and Peskoff, 1996). However, to date, no model has considered the effects of mobile and immobile buffers as well as the electric field associated with fixed surface charges on diadic cleft calcium movements. Although the influence of surface charge effects on sarcolemmal calcium binding has been examined previously (Bers et al., 1985), the effect of surface charge on the movement of calcium within the junctional space is unclear. The major problem with a full Nernst-Planck electrodiffusion and Poisson treatment of calcium movements over the "large" diadic space is the computational difficulty or "stiffness" of the system. Nevertheless, by assuming that the electric field is exponential from the surface, we have been able to construct a computer model that allows examination of the effect of surface charge and the electric field in the cardiac diad.

In this paper we compute the local $[Ca^{2+}]$ changes produced by DHPR gating to address the following questions: 1) During and after the opening of a DHPR, what local $[Ca^{2+}]$ levels are produced inside the diad? 2) What role does surface charge play? 3) How large are the gradients of $[Ca^{2+}]$ in the junctional space and what is the influence of diad diameter? 4) What is the relationship between the DHPR current and the local $[Ca^{2+}]$ level? Our results show that the surface charge has significant effects on the time course of calcium movements in the diad and causes local calcium changes to occur more rapidly than predicted from models that consider sarcolemmal calcium binding without field effects (Langer and Peskoff, 1996). In addition, our results suggest a possible explanation for the evolutionary divergence of cardiac and skeletal muscle types of E-C coupling. A preliminary account of some of this work has been presented (Soeller and Cannell, 1996).

*Received for publication 31 October 1996 and in final form 14 March 1997.*

Address reprint requests to Prof. M. B. Cannell, Department of Pharmacology and Clinical Pharmacology, St. George's Hospital Medical School, London SW17 0RE, England. Tel.: 44-181-725-5625; Fax: 44-181-725-3581; E-mail: mcannell@sghms.ac.uk.



0006-3495/97/07/97/15 $2.00

## METHODS

### Calcium movements

The viscosity of cytoplasm should reduce the diffusion coefficient for calcium in water ($D = 7 \times 10^{-6}$ cm$^2$ s$^{-1}$; Wang, 1953) by a factor of ~2 (Kushmeric and Podolsky,

1969). In the diadic space, the effective diffusion coefficient for radial transport will be further reduced by the presence of the "feet" structures (Sommer and Waugh, 1976), hindering calcium movement. Using dimensions for the array of feet structures reported from electron microscopy studies (i.e., a unit cell size of 31 × 31 $nm^2$ and a foot structure cross section of 27 × 27 $nm^2$; Saito et al., 1988), a tortuosity factor for transport in the radial direction of 0.4 can be estimated (see figure 12.8 in Crank, 1975). Therefore, the diffusion coefficient for calcium was taken as $1.4 \times 10^{-6}$ $cm^2\ s^{-1}$ in the radial direction in the diadic space ($D_r$) and $3.5 \times 10^{-6}$ $cm^2\ s^{-1}$ in the $z$ direction ($D_z$).

## Junctional geometry

The junction was modeled as a narrow cylindrical space formed by circular portions of the SR membrane and sarcolemmal membrane (see Fig. 1). The distance between these membranes is typically 15 nm (Fawcell and McNutt, 1969; Forbes and Sperelakis, 1982). The feet structures that span this "diadic gap" are also ~15 nm high (as determined from three-dimensional reconstruction; Radermacher et al., 1994). The width of the t-tubule is highly variable, with diameters between 60 nm and 200 nm (Forssmann and Girardier, 1970; Sommer and Johnson, 1979). The diad wraps around part of the t-tubule (Sommer and Johnson, 1979), and electron micrographs in the literature also suggest a large variation in diad size (e.g., Sommer and Waugh, 1976; Fawcell and McNutt, 1969; Forbes and Sperelakis, 1982). Without detailed morphometric analysis of the actual shape of a "typical" diad, we therefore modeled the diad as a circular region with diameters between 100 nm and 400 nm.

## Calcium binding by membranes

Assuming two sarcolemmal calcium-binding sites with concentrations of 85 nmol/mg sarcolemmal protein and 7 nmol/mg sarcolemmal protein (low- and high-affinity sites, respectively), with 7.5 g sarcolemmal protein/kg wet cells

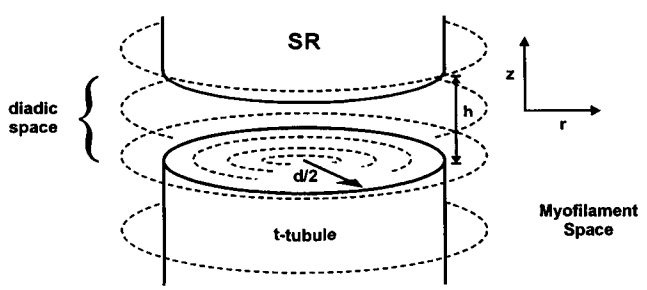


FIGURE 1 Diagrammatic sketch of the model geometry. The diadic region is the narrow cylindrical space between circular portions of the SR membrane and sarcolemmal membrane (t-tubule). The geometry is defined by the distance $h$ between these membranes and the diameter $d$ of the diadic gap. Polar coordinates were used in the computations, with the $z$ axis parallel to the axis of revolution and the radial coordinate measured orthogonal to this axis.

(Post and Langer, 1992), we can estimate 190 nmol calcium binding/mg protein. With a surface-to-volume ratio of 0.31 $\mu m^2/\mu m^3$ (Page, 1978), this binding would equate to $4.56 \times 10^{-20}$ $mol/\mu m^2$, giving 0.34 $nm^2$/binding site. The latter figure seems too small when phospholipid headgroups occupy ~0.6–0.9 $nm^2$ (Hope et al., 1985; Schieren et al., 1978). We therefore reduced the surface concentrations of both sarcolemmal membrane calcium-binding sites to 40% of the value calculated above. This gives a concentration of 76 nmol/mg, close to that measured in "gas dissected" membranes (Post and Langer, 1992).

Sites on the outer SR membrane occurred at a concentration of 19 μM/kg wet cells (Fabiato, 1983), giving a surface concentration of $1.3 \times 10^{-20}$ $mol/\mu m^2$, assuming a total surface area-to-volume ratio of 1.46 $\mu m^2/\mu m^3$ for rat ventricular myocytes (Bers, 1991). As the large RyR receptor will occupy a considerable portion of the SR membrane in the diad, the local density of binding sites should be lower when compared to regions without RyRs. Therefore, given the geometry of the RyR, 30% of the outer SR membrane area was assumed to be occupied by the RyR protein and therefore to be unable to contribute to calcium binding. Calcium binding by the RyR itself was ignored, as it is negligible in comparison to the binding sites provided by sarcolemmal phospholipids (and to a lesser extent SR phospholipids and other binding sites).

It is well known that lipid bilayers give rise to electrostatic effects due to the surface charge associated with the negatively charged phospholipid headgroups (McLaughlin et al., 1971; Langner et al., 1990). It has been shown (Bers et al., 1985) that surface binding of $[Ca^{2+}]$ to phospholipid headgroups on the sarcolemmal membrane can be described using the Gouy-Chapman theory of the diffuse double layer (Delahay, 1965). The Gouy-Chapman theory predicts an increased concentration of cations (the "diffuse double layer") in the immediate vicinity of a negatively charged plane as compared to the bulk solution. Thus surface binding constants based on the bulk ion concentrations will be quite different from the "true" association constants at the membrane. To take these effects into account, we calculated a system of local surface association constants that are in agreement with the binding behavior observed by Post and Langer (1992).

To calculate the amount of each ion species bound to a site on the membrane, we follow a general approach outlined previously (Bers et al., 1985). The amounts of ions bound at the membrane and surface potential were calculated from the following equations. First, the Graham equation (Delahay, 1965):

$$\sigma = 2\varepsilon_r\varepsilon_0 RT \sum_i c_{i,s} \quad \text{where } c_{i,s} = c_i \exp(-z_i\Phi_0) \quad (1)$$

where the surface charge $\sigma$ is related to the ion concentrations $c_{i,s}$. $\Phi_0$ is the nondimensional surface potential (note that $\Phi_0$ is related to the potential ($\Psi_0$) by $\Psi_0 = \Phi_0 \cdot kT/e$), $z_i$ is the valence number of ion species $i$, and $c_i$ is the bulk concentration of $i$.

The amount bound depends on the local surface concentration of the ion as well as all of the other ions competing for that site. For example, for calcium:

$$[CaB] = \frac{PL}{2}\left(\frac{k_{Ca}[Ca]}{1 + k_{Ca}[Ca] + k_{Na}[Na] + k_K[K] + k_H[H] + k_{Mg}[Mg]}\right) \quad (2)$$

where $PL$ is the total number of cation-binding sites. Similar equations specify the amount of ions of Na, K, Mg, and H bound to the membrane phospholipids. Finally, the binding of cations reduces the surface charge density,

$$\sigma = \sigma_t - (2[CaB] + 2[MgB] + [NaB] + [KB] + [HB]) \quad (3)$$

where the total charge density $\sigma_t$ is determined by the surface concentration of charged phospholipids. With correction for the proton concentration affecting the titration of amino groups on the phospholipids (Bers et al., 1985),

$$\sigma_t = PS + B + [(PE + PS)/(1 + k_{nH}[H])] \quad (4)$$

where PS is phosphatidylserine, PC phosphatidylcholine, PE phosphatidylethanolamine, and B unspecified calcium-binding sites.

Fig. 2 *A* shows the Scatchard plot of the sarcolemmal Ca binding (based on the values given by Post and Langer, 1992) plotted against bulk $[Ca^{2+}]$ concentration. The gray line in this figure shows the binding curve obtained from Gouy-Chapman theory (see above) with our choice of surface association constants. The membrane composition was

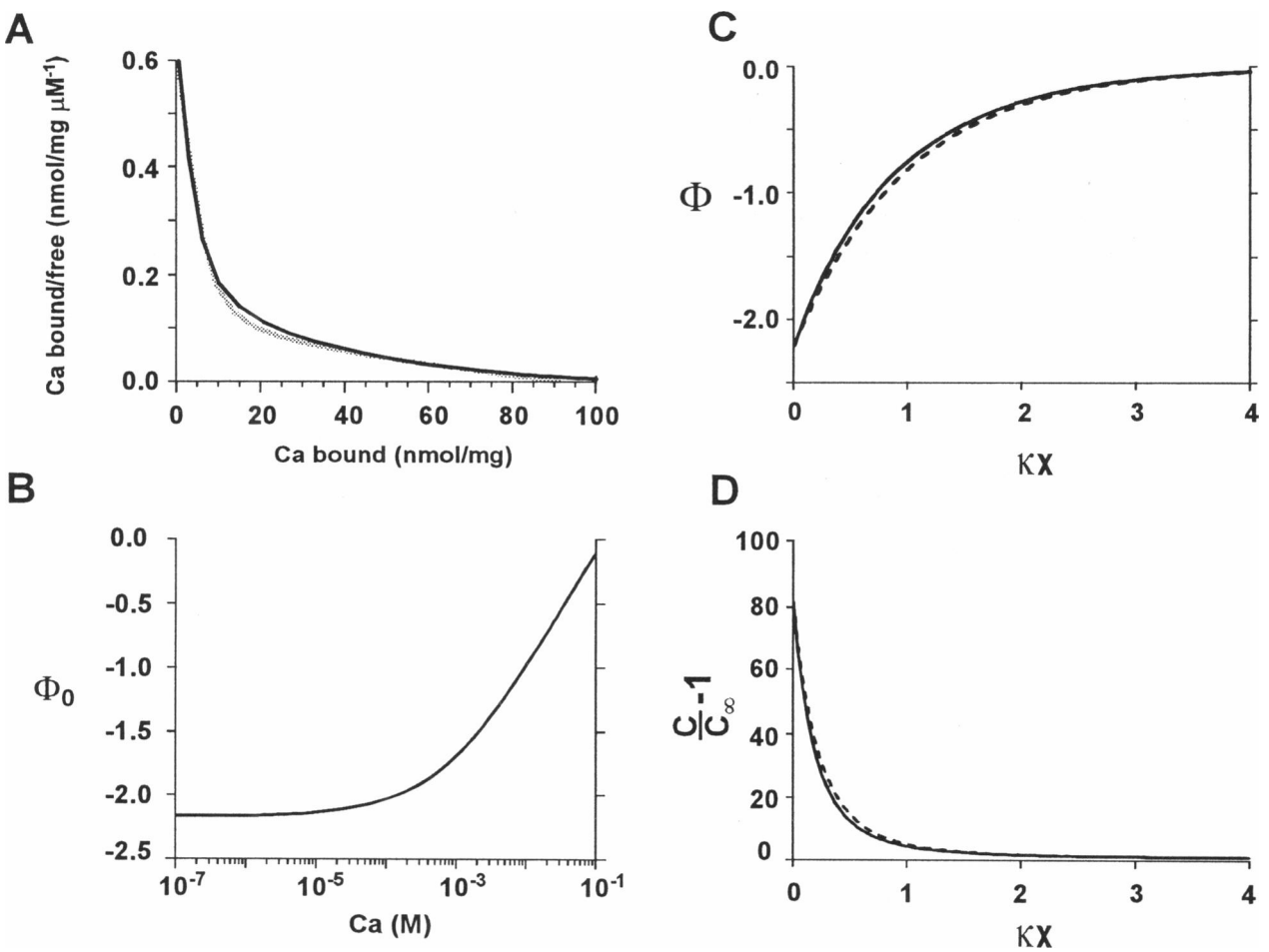


FIGURE 2 (*A*) Scatchard plot of sarcolemmal calcium binding. *Solid curve*: Binding curve assuming two classes of binding sites at concentrations of 85 nmol/mg sarcolemmal protein and 7 nmol/mg sarcolemmal protein with binding constants of 1 mM and 13 μM, respectively, without consideration of surface charge effects. *Gray curve*: Binding curve calculated including surface charge effects. This binding curve was calculated using a $K_d$ of 83 mM and 2.5 mM for the low- and high-affinity calcium binding, respectively, and surface binding constants for Na, K, Mg, and H binding were 1.6 M, 3.3 M, 166 mM, and 2.6 mM, respectively. The surface association constant for the deprotonation of amino groups $k_{NH}$ was $8 \times 10^5$ $M^{-1}$, which was chosen to fit the pH dependence of Ca binding (Bers et al., 1985). A total phospholipid surface concentration of 375 nmol/mg protein was used. The high-affinity binding site B was present at 10 nmol/mg protein. (*B*) Steady-state potential (in units of $e/kT$ or ~25 mV at 300K) at the sarcolemmal membrane as a function of bulk free $[Ca^{2+}]$. A nearly constant surface potential of ~55 mV was obtained for calcium concentrations smaller than 0.1 mM. (*C* and *D*) Approximation of the dependence of surface potential on distance from the membrane by an exponential. *Solid curves*: Potential (*C*) and relative concentration increase (*D*) above bulk value as a function of membrane distance computed from the monovalent solution (Eq. 12). *Dashed curves*: Potential (*C*) and relative concentration increase (*D*) computed using the exponential approximation (Eq. 13).

20% PS, 38% PE, and 38% PC (similar to values given in Bers et al., 1985), with unspecified binding sites (B) accounting for 4% of total binding (which was included to explain the high-affinity binding site identified by Post and Langer, 1992). We used typical physiological values for the composition of the cytosol, i.e., an aqueous solution with a concentration of 145 mM monovalent anions ($Cl^-$ and protein), 145 mM monovalent cations (140 mM $K^+$, 5 mM $Na^+$), and 0.5 mM $Mg^{2+}$ with varying amounts of calcium. It is apparent that our choice of surface association constants adequately describes sarcolemmal calcium binding as reported by Post and Langer (1992). Furthermore, the chosen surface association constants for binding of Mg (6 $M^{-1}$) and Ca (12 $M^{-1}$) are similar to those reported in the literature (Lau et al., 1981; McLaughlin et al., 1981).

Additional binding sites outside the diad space were provided by troponin, longitudinal SR, and mitochondria. The concentrations of these sites and their affinities are summarized in Table 1. Furthermore, as a mobile buffer, calmodulin and calcium-calmodulin were allowed to diffuse throughout the system (including the diad). Where possible, kinetic parameters for all of the classes of calcium-binding site were taken from the literature (see Table 1); however, for some sites no information about on and off rates could be found. In these cases a typical near-diffusion-limited on rate of 125 $\mu M^{-1}\ s^{-1}$ was assumed. The off rate was then obtained from the reported value of $K_d$. Calcium was assumed to bind to each of the above sites according to

$$Ca + B_i \underset{k_{off}}{\overset{k_{on}}{\rightleftharpoons}} B_iCa \tag{5}$$

for any site $B_i$. The net flux of calcium associated with binding to site $B_i$ is

$$F_i([Ca]) = k_{on}[Ca][B_i] - k_{off}[B_iCa] \tag{6}$$

## Electrodiffusion

To correctly describe $[Ca^{2+}]$ levels near charged membranes, an estimate of the potential distribution inside the double layer is necessary. The equilibrium shape of the potential can be obtained from the electrodiffusion equations (cf. Peskoff and Bers, 1988). The flux density $J_i$ of the $i$th ion species is thereby related to the ion density $c_i$ and the nondimensional electric potential $\Phi = \Psi/(e/kT)$ by the Nernst-Planck electrodiffusion equation:

$$J_{i,x} = -D_{i,x}\left(\frac{dc_i}{dx} + z_i c_i \frac{d\phi}{dx}\right) \tag{7}$$

where $D_i$ and $z_i$ are the diffusion coefficient and the valence of the $i$th ion species, respectively. $x$ is the direction within the coordinate system, which in this model is $r$ and $z$. At equilibrium, $J_i \equiv 0$, and therefore

$$c_i(z) = C_i(0)\exp(-z_i\Phi(z)) \tag{8}$$

if the membrane is planar and of (effective) infinite extent. The resulting field distribution can be obtained as the solution of the Poisson equation, which relates the Laplacian of the potential to the net charge density:

$$\frac{d^2\Phi}{dz^2} = -\frac{e^2}{\varepsilon_r\varepsilon_0 kT}\sum_i z_i c_i \tag{9}$$

Considering $Ca^{2+}$, $K^+$, $Na^+$, $Mg^{2+}$, and $H^+$ as well as monovalent anions (mainly $Cl^-$),

$$\frac{d^2\Phi}{dz^2} = -\frac{e^2[Cl^-]}{\varepsilon_r\varepsilon_0 kT}(\alpha\exp(-2\Phi) + (1-\alpha)\exp(-\Phi) - \exp(\Phi)) \tag{10}$$

where $\alpha = 2([Ca] + [Mg])/[Cl]$ and is the ratio of divalent to monovalent anion concentration (compare Bers et al., 1985). From this equation, it is clear that for moderate $[Ca^{2+}]$ levels (e.g., $[Ca^{2+}] < 0.1$ mM when $[Mg] \approx 0.5$ mM; see Fig. 2), the monovalent form of the potential ($\alpha = 0$) will be a good approximation, giving

$$\frac{d^2\Phi}{dx^2} = \frac{1}{\kappa^2}\sinh(\Phi(x)) \tag{11}$$

where

$$1/\kappa^2 = 2e^2[Cl^-]/\varepsilon_r\varepsilon_0 kT$$

which is the square of the Debye length ($1/\kappa$). The solution of Eq. 12 for a monovalent 1–1 electrolyte predicted from

**TABLE 1 Additional calcium buffers incorporated in the model**

| Calcium buffer | Concentration and dissociation constant ($K_d$) | Reference |
|---|---|---|
| Troponin Ca-specific sites | Resting concentration 70 $\mu$M<br>$K_d$ 2 $\mu$M | Fabiato (1983) |
| Troponin Ca/Mg sites | Resting concentration 0.14 mM<br>$K_d$ 2.5 nM (and $K_{d_{Mg}}$ 30 $\mu$M) | Holroyde et al. (1980) |
| Calmodulin high-aff. sites | Resting concentration 12 $\mu$M<br>$K_d$ 1.9 $\mu$M | Fabiato (1983) |
| Calmodulin low-aff. sites | Resting concentration 12 $\mu$M<br>$K_d$ 34.5 $\mu$M | Fabiato (1983) |
| Calmodulin diffusion coefficient | $D_{CM} = 0.1 \times D_{Ca}$ | From molecular weight and Smith et al. (1996) |
| Mitochondria | Local concentration 100 $\mu$M<br>$K_d$ 3.5 $\mu$M | Carafoli and Lehninger (1971)<br>Bers (1991) |

Gouy-Chapman theory (Delahay, 1965; Langner et al., 1990) is

$$\Phi(x) = 2 \ln \frac{1 + \alpha \exp(-\kappa x)}{1 - \alpha \exp(-\kappa x)} \quad (12)$$

where

$$\alpha = \frac{\exp(\Phi(0)/2) - 1}{\exp(\Phi(0)/2) + 1}$$

which is reasonably approximated by a single exponential for small $\Phi_0 = \Phi(0)$:

$$\Phi(x) = \Phi_0 \exp(-\kappa x) \quad (13)$$

Fig. 2 *C* shows that the exponential approximation is adequate for $\Phi_0 = -2.2$, which is representative for sarcolemmal binding at $[Ca^{2+}] \leq 0.1$ mM (Fig. 2 *B*). Fig. 2 *D* shows that the exponential assumption for the concentration profile within the double layer is reasonable. Based on this one-dimensional equilibrium solution, we incorporate the presence of the double layer into the numerical scheme with the following assumptions: 1) The one-dimensional solution can be used in the presence of radial $[Ca^{2+}]$ gradients, provided the electric field curvature is small. 2) The monovalent ion fluxes are small. The first assumption is reasonable because the radius of curvature of biological membranes is generally much larger than the Debye length (which was set to 1 nm in our computations). Moreover, perturbations in the electric field due to the calcium movements will be small in the presence of large concentrations of monovalent ions, because the peak $[Ca^{2+}]$ is less than 0.1 mM (see Results) compared to other ions at ~150 mM. Similarly, the second assumption seems reasonable when we consider that the small calcium flux is balanced by equivalent fluxes of the other ions, which are small as compared to the total ion concentration of those ions. Within these assumptions, the electrodiffusion equation (with binding) to solve is

$$\frac{\partial[\mathrm{Ca}]}{\partial t} = -\vec{\nabla} \cdot \vec{J} + \sum_i F_i([\mathrm{Ca}]) \quad (14)$$

in which the calcium flux components in the radial and axial directions are

$$J_r = -D_r \cdot \frac{\partial[\mathrm{Ca}]}{\partial r} \quad (15)$$

and

$$J_z = -D_z \left( \frac{\partial[\mathrm{Ca}]}{\partial z} + 2[\mathrm{Ca}] \frac{d\Phi}{dz} \right) \quad (16)$$

The discretization of this partial differential problem was carried out in a cylindrical coordinate system as described below.

## Boundary conditions

Although membranes curve gently away from the edge of the diad space, such a geometry would be impossible to reproduce with a cylindrical computational grid. For convenience, we therefore assumed square edges (as shown in Figs. 1 and 5) and prevented fluxes (normal to the membrane surface) over the surfaces of the elements at these corners. This effectively reproduced the required uniform electric field. All simulations started with a uniform calcium distribution (100 nM) and the equilibrium levels of calcium occupancy of all buffers. At the boundary of the computational space (at $r$ and $z = 2$ $\mu$m), $\partial[\mathrm{Ca}]/\partial t = 0$.

## L-type calcium channel

The calcium channel was modeled as a (variable) calcium flux with a maximum single-channel current of 0.2 pA at +10 mV (Rose et al., 1992). For the calculations presented here, the channel was placed in the center of the diad to give the problem radial symmetry and thereby allow the use of cylindrical geometry (see below). Because lipid surface charge has little effect on permeation of t-tubule calcium channels (Coronado and Affolter, 1986), the intracellular mouth of the channel must be largely outside the electric field. We therefore assumed that the transsarcolemmal calcium influx entered the diadic space 3 nm above the sarcolemmal membrane surface.

## Numerical solution of diffusion-reaction equations

Taking the cylindrical symmetry of the problem into account, the system of equations was solved on a two-dimensional nonlinear grid. The minimum grid element size was 0.1 nm high and 5 nm wide in the vertical ($z$) and radial ($r$) directions, respectively. Independent tests showed that the chosen grid geometry was sufficiently fine for solving the systems of equations described here. The grid covered a radial distance of 2 $\mu$m and extended 2 $\mu$m in each axial direction with the diad in the center of the model space, giving a total of 1968 grid points. At each grid point, all of the relevant differential equations were integrated with a fully implicit backward-difference predictor-corrector scheme (see Cannell and Allen, 1984, for description of a closely related nonlinear finite-difference cylindrical discretization problem). The program was compiled using double-precision variables (to eliminate truncation problems) in 64-bit Fortran77 and solved with an Indigo$^2$ workstation with 128 Mbytes of memory (Silicon Graphics, Mountain View, CA). Starting integration step sizes were $\sim 10^{-14}$ s.

# RESULTS

Fig. 3 shows the effect of including various classes of binding site and the electric field on the calculated $[Ca^{2+}]$ levels associated with the continuous activation of a 0.2-pA

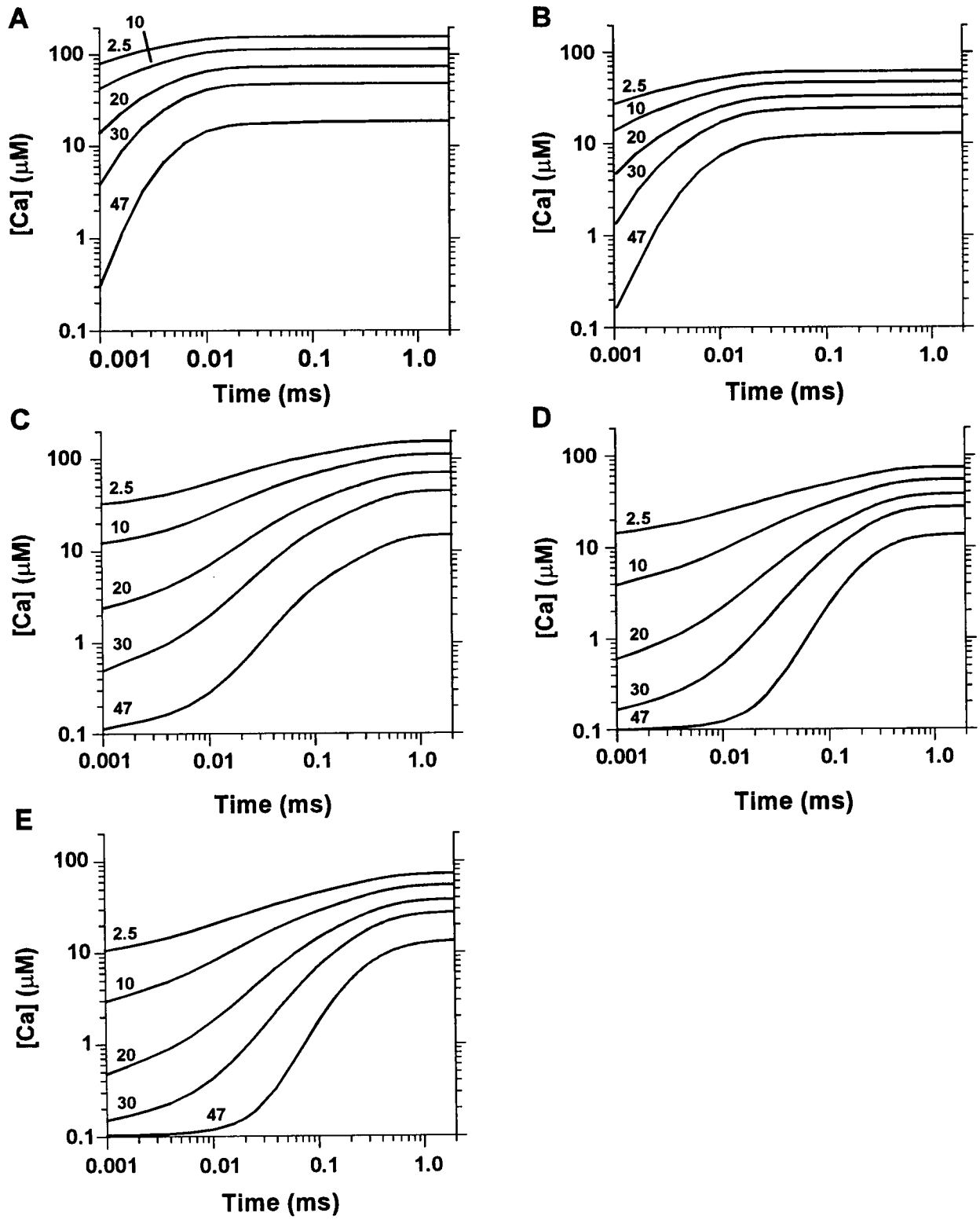


FIGURE 3 Effect of including various classes of binding sites and surface charge on calculated $[Ca^{2+}]$ levels as a function of time from the start of a continuous DHPR calcium influx (0.2 pA). The time course of $[Ca^{2+}]$ in a diad 100 nm across is shown for various radial distances from the center (marked on the curves in nm) and 4 nm below the SR membrane. (*A*) Calculated time course without including any calcium-binding sites or surface charge. (*B*) The effect of including surface charge, which results in a decrease of $[Ca^{2+}]$ levels at all times and locations. (*C*) The effect of including sarcolemmal calcium-binding sites (but without surface charge). This results in a marked increase in the rise time of $[Ca^{2+}]$, but with no change in steady-state levels compared to *A*. (*D*) Result of including sarcolemmal calcium binding and surface charge effects. The off-rate constants for the sarcolemmal binding sites had to be increased above those used to calculate the results shown in *C* to reproduce the binding dependence on bulk $[Ca^{2+}]$ levels (see Methods). (*E*) Effect of including all other binding sites (mitochondria, troponin, calmodulin, and SR membranes).

calcium influx at the center of the diad. Fig. 3 *A* shows the time course of the increase in $[Ca^{2+}]$ at varying positions from the center of a 100-nm-diameter diad without calcium buffers or surface charge effects. In general, near-steady levels of $[Ca^{2+}]$ are achieved in 0.01 ms, although the absolute level has a strong dependence on radial position. Opposite the DHPR, the steady-state level of $[Ca^{2+}]$ was 158 $\mu$M, which decreased with radial distance to 19 $\mu$M at the edge of the diad. The inclusion of the surface charge (Fig. 3 *B*) results in a marked decrease in $[Ca^{2+}]$ levels at all times and positions with the diad (reaching 63 $\mu$M at the center of the diad in the steady state), as well as an approximately fivefold increase in the rise time of $[Ca^{2+}]$.

Fig. 3 *C* illustrates the effects of including sarcolemmal calcium-binding sites within the diad (but without electric field effects) and is therefore analogous to the model presented recently by Langer and Peskoff (1996). In general agreement with the conclusions of Langer and Peskoff (1996), the inclusion of sarcolemmal calcium-binding sites results in a marked reduction in the rate of rise of $[Ca^{2+}]$, but with no effect on steady-state levels. At the edge of the diad, the time taken to reach 1 $\mu$M and 10 $\mu$M was ~0.033 ms and 0.4 ms, respectively. However, the model presented here is different from that presented by Langer and Peskoff (1996) because it uses a slightly lower rate of calcium influx and predicts steady-state $[Ca^{2+}]$ levels that are about an order of magnitude lower. We have no explanation for the latter difference. Fig. 3 *D* shows that the effects of including sarcolemmal calcium binding and the electric fields combine to produce a steady-state $[Ca^{2+}]$ of 73 $\mu$M at the center of the diad. (It should be noted that for this simulation, the off-rate constants for the sarcolemmal calcium-binding sites had to be increased above those used for Fig. 3 *C* to reproduce the bulk calcium dependence of sarcolemmal calcium binding; see Methods). The time taken to reach 1 $\mu$M and 10 $\mu$M was ~0.06 ms and 0.4 ms, respectively, at the edge of the diad. However, the electric field introduced complicated effects on the time course of $[Ca^{2+}]$ changes, because it accelerated the approach to steady-state levels while slowing the initial rate of rise of $[Ca^{2+}]$ at the edge of the diad. Such effects may be related to the changes in the altered binding kinetics of the sarcolemmal calcium-binding sites as well as the introduction of steep calcium gradients between the SR and sarcolemmal membranes. The model of Langer and Peskoff (1996) suggests a slower rate of rise of $[Ca^{2+}]$, but this is partly due to the assumption of instantaneous calcium binding by the phospholipids in that model. Surface charge has little effect on the steady-state $[Ca^{2+}]$ at the edge of the diad, but reduces the $[Ca^{2+}]$ in the center of the diad (compared to Fig. 3 *C*), thereby reducing the gradient of $[Ca^{2+}]$ across the diad.

Fig. 3 *E* shows the effect of including all other binding sites in the model (namely calcium binding by mitochondria, troponin, calmodulin, and SR membranes). It is clear that these extra calcium-binding sites have only minor effects on the $[Ca^{2+}]$ levels within the diad. Thus, as far as diadic $[Ca^{2+}]$ levels are concerned, the sarcolemmal calcium-binding sites (and the changes in electric field that they produce) are the most important calcium-binding sites.

Fig. 4 shows the effect of including different classes of binding sites and the electric field on the decay of $[Ca^{2+}]$ levels after a 0.3-ms period of calcium influx. The arrangement of panels is similar to that in Fig. 3. Fig. 4 *A* shows the rapid decay of elevated $[Ca^{2+}]$ levels at various positions across the diad without calcium buffers and surface charge effects. In less than 50 $\mu$s, $[Ca^{2+}]$ levels have decreased by an order of magnitude everywhere across the diad. Fig. 4 *B* shows the effect of surface charge, and there is still an initial fast decay with a time constant only slightly longer than in Fig. 4 *A*, whereas $[Ca^{2+}]$ levels at all times are lower than in Fig. 4 *A*. Fig. 4 *C* shows the effects of including sarcolemmal binding sites (same conditions as in Fig. 3 *C*). It is apparent that the radial gradient at all times is maintained, an effect that is due to the nonuniform levels of calcium binding across the diad and the slower release of calcium from the binding sites. In addition, the decay is markedly slowed, taking more than 2 ms to fall from ~10 $\mu$M to ~1 $\mu$M. This is in general agreement with the results of Langer and Peskoff (1996). The combined effect of surface charge and sarcolemmal calcium binding are shown in Fig. 4 *D*. Again, the effects of surface charge and calcium binding are somewhat additive; the presence of the surface charge reduced the radial gradients, whereas the binding slows down the decay. Compared to Fig. 4 *C*, however, the decay is nearly linear in the log-log plot, and so can be approximated by a power law dependence on time. It is notable that it takes ~0.8 ms (which is 1.1 ms from the start of the simulation) for $[Ca^{2+}]$ levels to decrease to 1 $\mu$M, whereas it takes up to 2 ms (at the center of the diad) in Fig. 4 *C* for $[Ca^{2+}]$ to fall to the same level. Fig. 4 *E* shows the effect of including all of the other binding sites. As seen in Fig. 3 *E*, the effects of the other buffers are minor when compared to sarcolemmal buffering. However, these buffers slightly slow the decay to resting levels, and it now takes ~5 ms to return to near-resting levels. This effect can be explained by the reduction in the effective diffusion coefficient for calcium in the cytoplasm by the cytoplasmic buffers (see Cannell and Allen, 1984), impeding the loss of calcium from the diad. These results emphasize the importance of including surface charge effects for calculating the $[Ca^{2+}]$ levels in the narrow diadic space after calcium influx via a channel.

Fig. 5 shows contour plots of the spatial distribution of $[Ca^{2+}]$ levels in the diadic space during and after termination of a 0.2-pA calcium influx lasting for 0.3 ms. As shown in Fig. 5 *A*, $Ca^{2+}$ spreads across the diadic space rapidly. It is notable that the gradients of $[Ca^{2+}]$ are not hemispherical during the initial phase of release, as has been modeled by others (e.g., Simon and Linas, 1985; Stern, 1992). Instead, the gradient of $[Ca^{2+}]$ resembles an "omega" shape as calcium is absorbed onto the membrane calcium-binding sites. This effect is also accentuated by the mouth of the calcium channel being placed 3 nm above the membrane (as required for surface charge to have no effect on single-

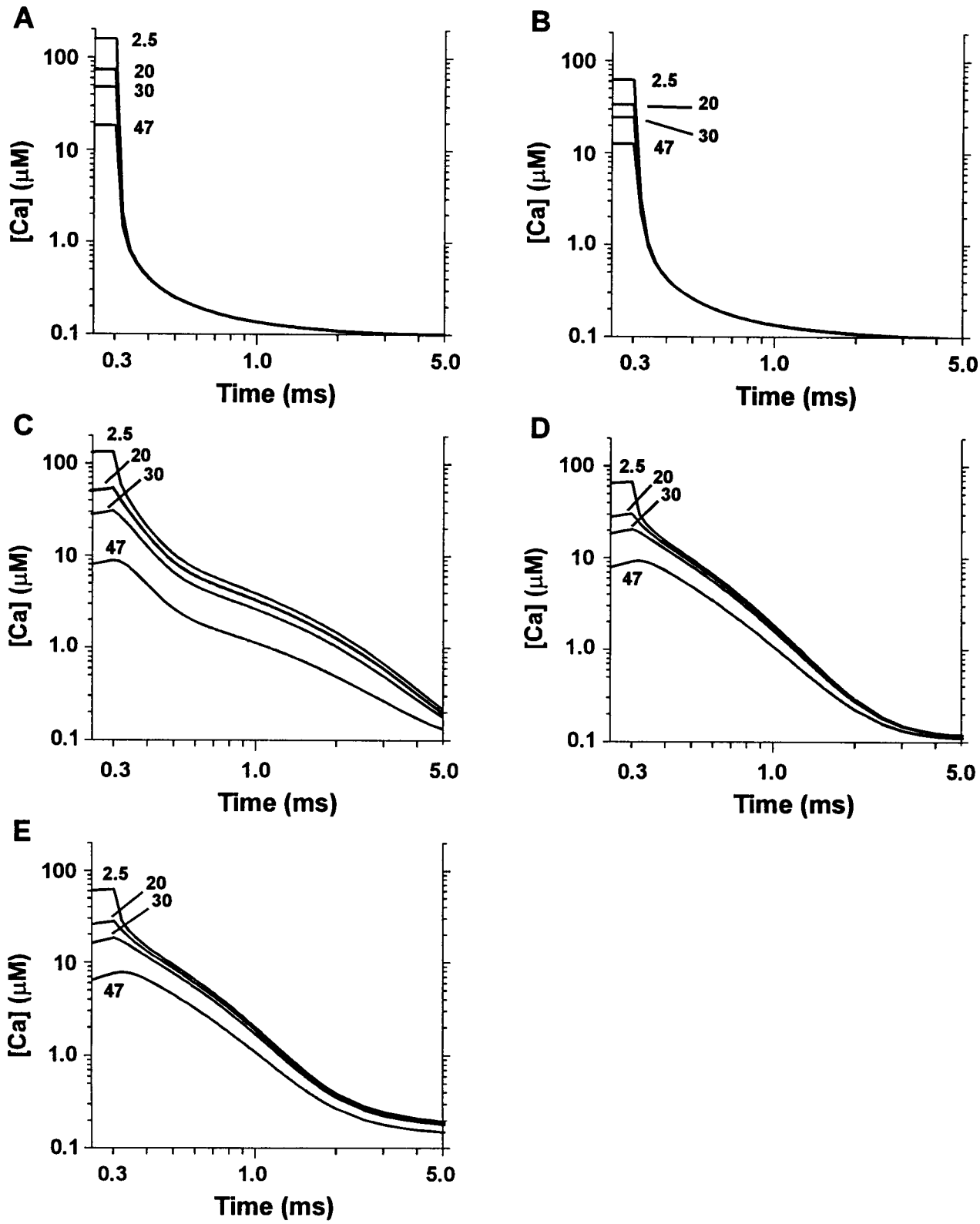


FIGURE 4 Effect of including various classes of binding sites and surface charge on calculated $[Ca^{2+}]$ levels as a function of time from the start of DHPR calcium influx (0.2 pA), which lasted 300 $\mu$s. Diad geometry as in Fig. 3. Results are shown for various radial distances from the center (written on the curves in nm) and 4 nm below the SR membrane. (*A*) Calculated time course without including any calcium-binding sites and surface charge. (*B*) Effect of including surface charge. Note the decrease in $[Ca^{2+}]$ levels at all times and locations. (*C*) Effect of including sarcolemmal calcium-binding sites (but without surface charge). This results in a marked increase in the decay time of $[Ca^{2+}]$. (*D*) Result of including sarcolemmal calcium binding and surface charge effects. The off-rate constant correction is as in Fig. 3 *D*. (*E*) Effect of including all other binding sites (mitochondria, troponin, calmodulin, and SR membranes).

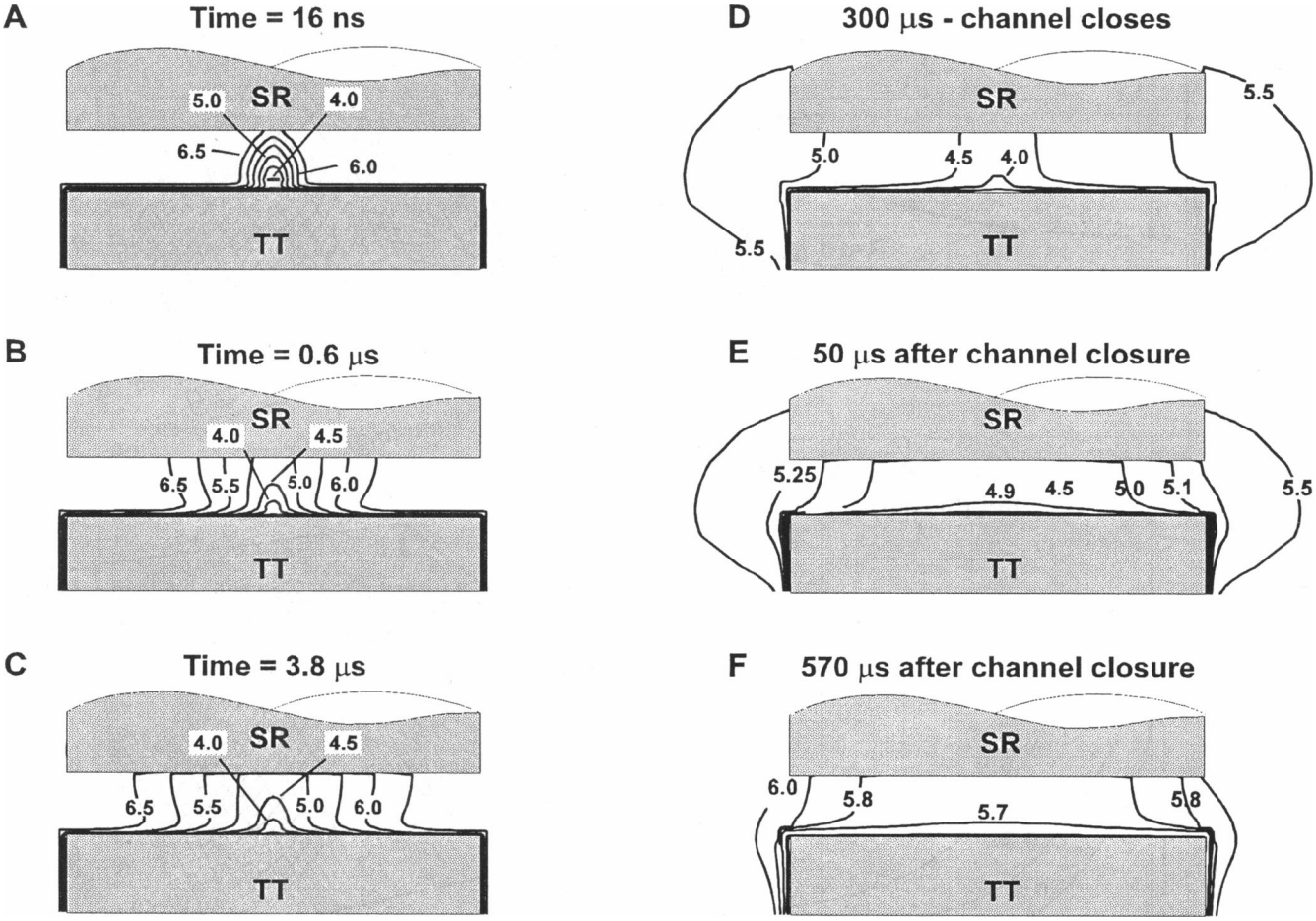


FIGURE 5 Contour plots of the spatial distribution of $[Ca^{2+}]$ in the diad (diameter 100 nm) at various times from the start of DHPR calcium influx (0.2 pA), which terminated after 300 μs. All calcium-binding sites (see Table 1) and the electric field were included in the simulation. The numbers at the contour lines indicate the computed $[Ca^{2+}]$ in pCa units. (*A*) Initial distribution shortly after the start of sarcolemmal influx. (*B* and *C*) As higher levels of $[Ca^{2+}]$ spread throughout the diad, the distribution resembles an "omega" shape. (*D*) At the time of DHPR channel closure, $[Ca^{2+}]$ levels in the diad have increased to 0.03 at the diad edge and 0.1 mM in the center. (*E* and *F*) After the calcium influx was terminated, $[Ca^{2+}]$ levels and radial gradients dissipated quickly.

channel current). The surface charge also results in an elevation of $[Ca^{2+}]$ above the nearby cytosolic levels within the Debye layer at all times, as seen as a "rim" of higher $[Ca^{2+}]$ levels around the t-tubule membrane. It is notable that $[Ca^{2+}]$ increases to 0.03–0.1 mM in the vicinity of the calcium channel in a few microseconds (Fig. 5, *B* and *C*), and these levels eventually occupy a significant fraction of the diadic space (Fig. 5 *D*). Whereas radial $[Ca^{2+}]$ gradients are significant (even in the steady state), the transgap $[Ca^{2+}]$ gradients are less significant, especially near the SR membrane. (Note that the slight roughness of the contours outside the diad arises solely from inability of the contouring program to deal with the irregular mesh of data points and the small gradients of $[Ca^{2+}]$ in that region.) Fig. 6 *A* shows the steady-state $[Ca^{2+}]$ levels as a function of the distance from the SR membrane at various radial distances from the center of the diad. It therefore follows that the $[Ca^{2+}]$ level detected by the RyR sensing site will be more sensitive to radial position than to height within the gap (see Cannell and Soeller, 1997). Fig. 6 *B* shows the time course of $[Ca^{2+}]$ changes for periods of sarcolemmal calcium influx of 0.1, 0.3, and 0.9 ms for the duration of the plot (4 ms) at a point 4 nm from the SR membrane directly opposite the DHPR. Note that the time course of the decline of $[Ca^{2+}]$ to 1 μM is quite similar after termination of sarcolemmal calcium influx. From this semilogarithmic plot it is clear that the time course of decline of $[Ca^{2+}]$ is not exponential. As the $[Ca^{2+}]$ levels approach their steady-state level during the DHPR opening, there is an increase in the amplitude of a very slow phase of decline. After a DHPR opening that resulted in near-steady-state conditions (0.9 ms), this apparent "tail" of $[Ca^{2+}]$ reached a level of ~0.4 μM at 4 ms. This "tail" was due to calcium release from the sarcolemmal calcium-binding sites. For all three open times, an initial fast decay of $[Ca^{2+}]$ to ~10 μM is followed by a slower decay to submicromolar levels in ≤1.2 ms after channel closure. This result shows that $[Ca^{2+}]$ levels within the diad will respond quickly to termination of calcium influx and

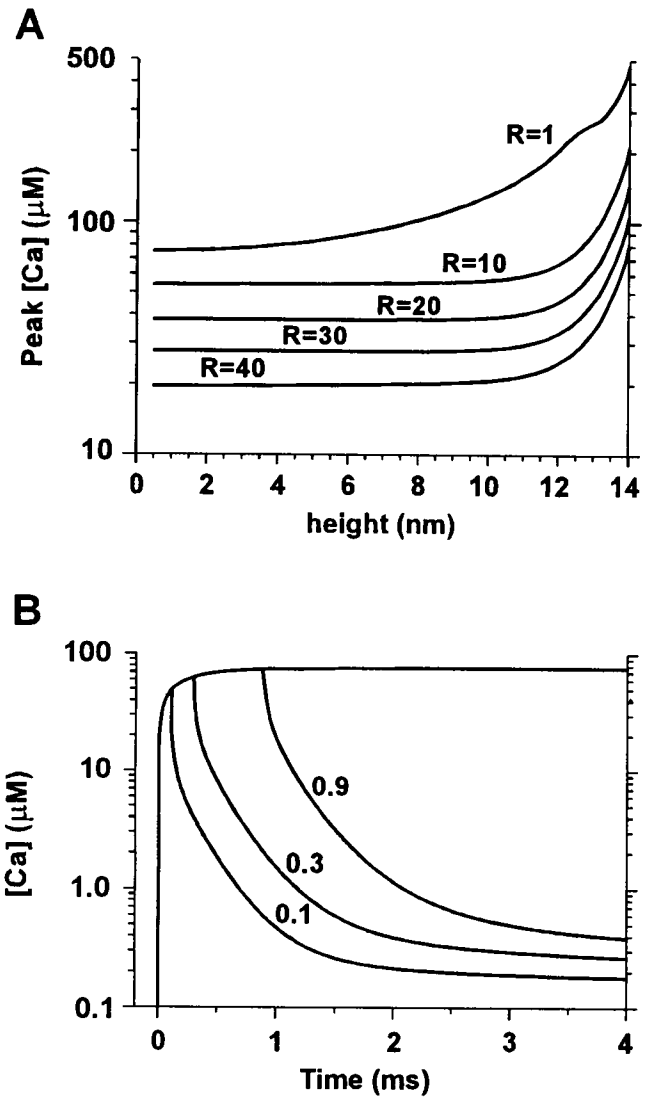


FIGURE 6 (*A*) Steady-state $[Ca^{2+}]$ levels in the diad as a function of distance from the SR membrane (DHPR influx magnitude and diad geometry as in the previous figure). The $[Ca^{2+}]$ levels are plotted for various radial distances (in nm) from the center as indicated on the curves. Apart from the $[Ca^{2+}]$ gradient adjacent to the sarcolemmal membrane (due to the presence of the surface charge), significant gradients toward the SR membrane are only observed in the immediate vicinity of the DHPR. The very high $[Ca^{2+}]$ levels in the double layer itself (14–15 nm from the SR) have been excluded from the plot for clarity. (*B*) Time course of $[Ca^{2+}]$ in response to a DHPR calcium influx of fixed duration of 0.1, 0.3, 0.9, and 4 ms at a point located 4 nm from the SR membrane. Curves are labeled with DHPR influx duration in ms. The unlabeled curve is the $[Ca^{2+}]$ time course for continuous DHPR calcium influx.

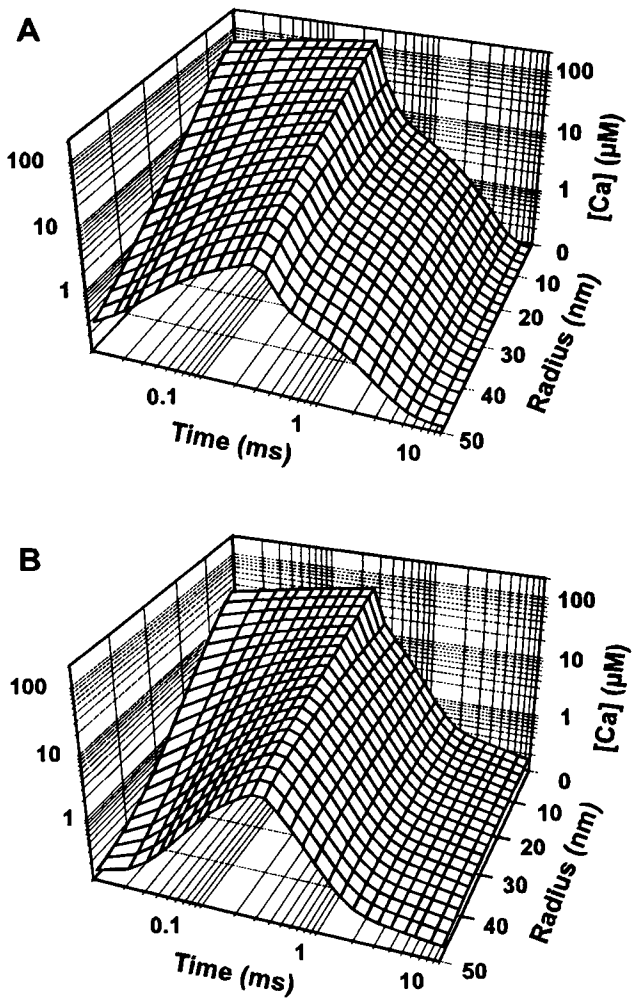


FIGURE 7 Surface plots of $[Ca^{2+}]$ in the diad with and without surface charge effects. $[Ca^{2+}]$ is shown for a diad 15 nm high and 100 nm across as a function of radius and time since the start of calcium influx. (*A*) $[Ca^{2+}]$ levels, computed including calcium binding (but without considering surface charge effects; see Figs. 3 *C* and 4 *C*). (*B*) $[Ca^{2+}]$ levels, where all calcium-binding sites (sarcolemmal membrane, SR membrane, troponin, calmodulin, and mitochondria) and surface charge effects have been included in the calculation. Note the lower $[Ca^{2+}]$ levels at all times for any given radial distance relative to those in *A*. Although initially the radial gradients in *B* are larger, at the time the DHPR channel closes, the radial gradient is smaller when surface charge effects are included. After the DHPR channel closes, the decay to resting $[Ca^{2+}]$ levels is faster when the electric field is included.

can help explain why termination of calcium influx results in a marked reduction in SR calcium release (e.g., Cannell et al., 1987, 1995; Isenberg and Han, 1994).

To further clarify some of the differences between these simulations and those of Langer and Peskoff (1996), Fig. 7 presents our data as surface plots of the time course of $[Ca^{2+}]$ level versus radial distance. Fig. 7 *A* shows the $[Ca^{2+}]$ transient at a height 4 nm from the SR membrane, where sarcolemmal calcium binding (but no surface charge effects; compare Figs. 3 *C* and 4 *C*) has been included, whereas in Fig. 7 *B* all binding sites and surface charge effects have been included. As described previously, the inclusion of surface charge effects results in lower $[Ca^{2+}]$ levels at all times, and the decay is faster after influx termination. Whereas at very early times (~1 μs) the radial gradient is increased by surface charge, at typical DHPR open times (~0.3 ms; see Rose et al., 1992) the gradient is reduced by surface charge. In connection with this point, it should be noted that this result is not due to our assumption

of negligible radial electric fields. In fact, the differences in surface potential across the diad are small (≤5%). In summary, we find that surface binding and the electric field have significant effects on the distribution of $[Ca^{2+}]$ within the diad, and all subsequent calculations shown here will include these factors.

## Effect of diad diameter

Because the diameter of the diadic region is variable, we have also calculated the time course of $[Ca^{2+}]$ for larger clefts (Fig. 8 compares 100-nm and 400-nm diads). The left-hand sides of Fig. 8, *A* and *B*, show the increase in $[Ca^{2+}]$ levels during the first 300 μs of a DHPR opening. In the central region of the diad ($r \leq 45$ nm), increasing the diameter has little effect on the time course of the rise in $[Ca^{2+}]$. Therefore, increasing the diameter of the diad (above 100 nm) will have minor effects on the $[Ca^{2+}]$ levels reached during the majority of DHPR open times. The panels on the right show the decay of $[Ca^{2+}]$ levels against time (after channel closure). Increasing the diad diameter has minor effects on the initial time course of the decline in $[Ca^{2+}]$. However, at later times after DHPR closure ($t \geq 1$ ms), the decline of $[Ca^{2+}]$ is slowed in larger diads. This effect is due to the larger total amount of phospholipid binding in the larger diad. As far as tight control of activation of CICR by the DHPR activity is concerned, large diads will therefore be disadvantageous, as accumulation of $[Ca^{2+}]$ in the diad is increased by increasing diad diameter. In Fig. 8, only radial distances up to 45 nm are shown (for straightforward comparison with a 100-nm diad). The full radial dependence for larger diads is shown in surface plots in Fig. 9 for diads measuring 200 nm and 400 nm across. In the case of the larger diads (200–400 nm), the increase and decay of $[Ca^{2+}]$ levels at the edge of the diad are significantly delayed when compared to the center. Furthermore, peak $[Ca^{2+}]$ levels at the edge of the 400-nm diad are below 1 μM, so that there would be an additional penalty for CICR associated with such large diads, as the majority of SR release channels (i.e., those near the edge of a large diad)

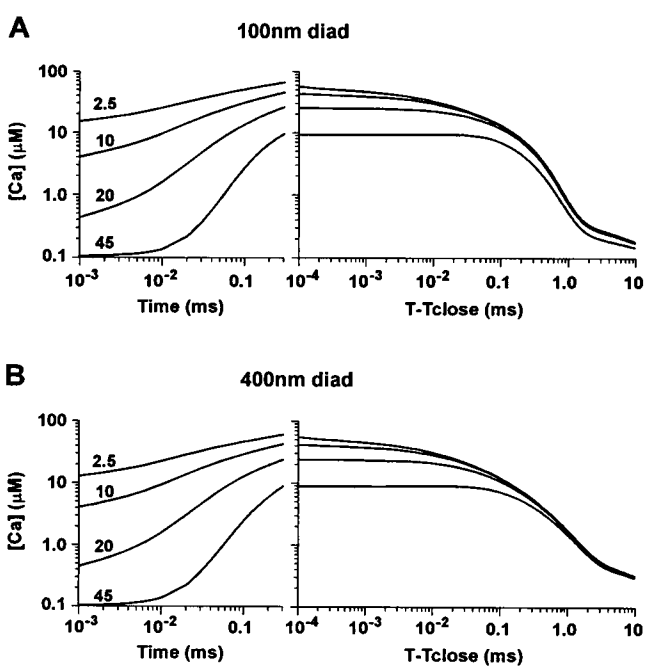


FIGURE 8 Time course of $[Ca^{2+}]$ at various distances from the center (marked at the curves in nm) in diads of different diameter. All curves correspond to points 4 nm above the SR membrane. (*A*) The $[Ca^{2+}]$ transient in a diad 100 nm across. Note that in the right half of the panel the time course is plotted as a function of time since the DHPR channel closed (0.3 ms). (*B*) $[Ca^{2+}]$ in a diad 400 nm across. Note the change in the time course of decline of $[Ca^{2+}]$ compared to *A*.

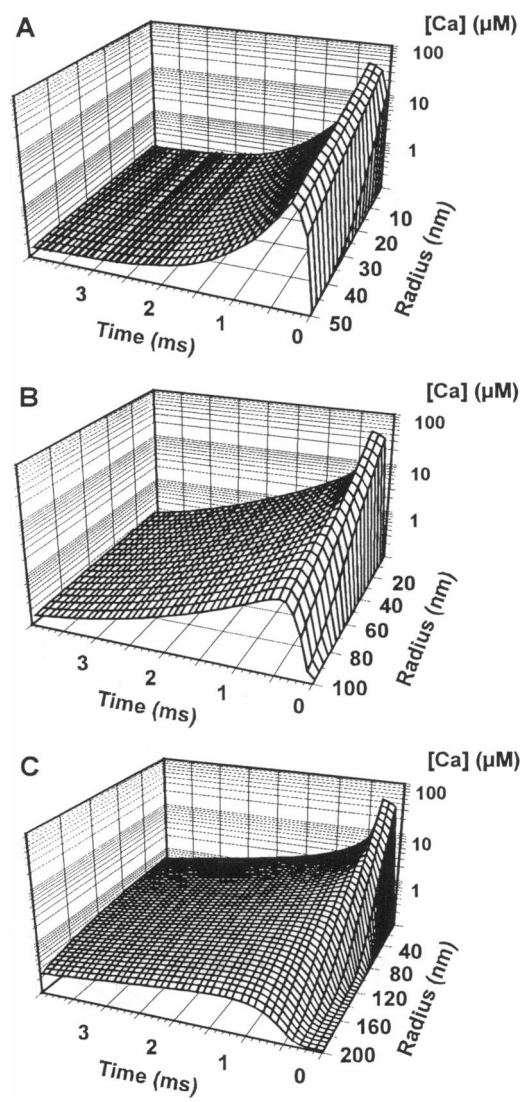


FIGURE 9 Surface plots of $[Ca^{2+}]$ 4 nm from the SR membrane for various different diad diameters. The DHPR calcium influx was 0.2 pA and lasted for 0.3 ms. (*A*) A 100-nm diad. The rapid decay of $[Ca^{2+}]$ levels after the DHPR closed is apparent. (*B*) A 200-nm diad. Note that the initial decay of $[Ca^{2+}]$ after DHPR closure is slower than that shown in *A*. (*C*) Time course of $[Ca^{2+}]$ changes in a 400-nm-diameter diad. Note the increased "apparent buffering" relative to the results shown in *A* and *B*.

would be barely activated. In other words, for efficient and responsive E-C coupling, several narrow diads (or an elliptical diad with a small minor axis and long major axis) would be advantageous (see Discussion).

### Dependence on calcium current amplitude

The amplitude of the calcium influx through the sarcolemmal DHPR will vary according to the membrane potential and external calcium concentration. Calculations performed with various values of the DHPR current suggest a near-linear dependence of the observed $[Ca^{2+}]$ levels on this parameter. This point is illustrated in Fig. 10, where results for influx amplitudes varying between 25 fA and 0.2 pA are summarized. In Fig. 10 *A*, the time course of the $[Ca^{2+}]$ change in the diad is plotted for the minimum (25 fA) and intermediate (0.1 pA) DHPR currents that have been examined in this study. Although there is a marked difference in the absolute level of $[Ca^{2+}]$ reached at any time, the time courses were very similar when normalized. This point is emphasized by the graphs shown in Fig. 10 *B*, which show that the $[Ca^{2+}]$ levels at two points in the diad have a near-linear dependence on the DHPR channel current. In summary, our model supports the idea (Stern, 1992; Santana et al., 1996) that the local $[Ca^{2+}]$ (at a given point within the diad) is approximately proportional to the single-channel

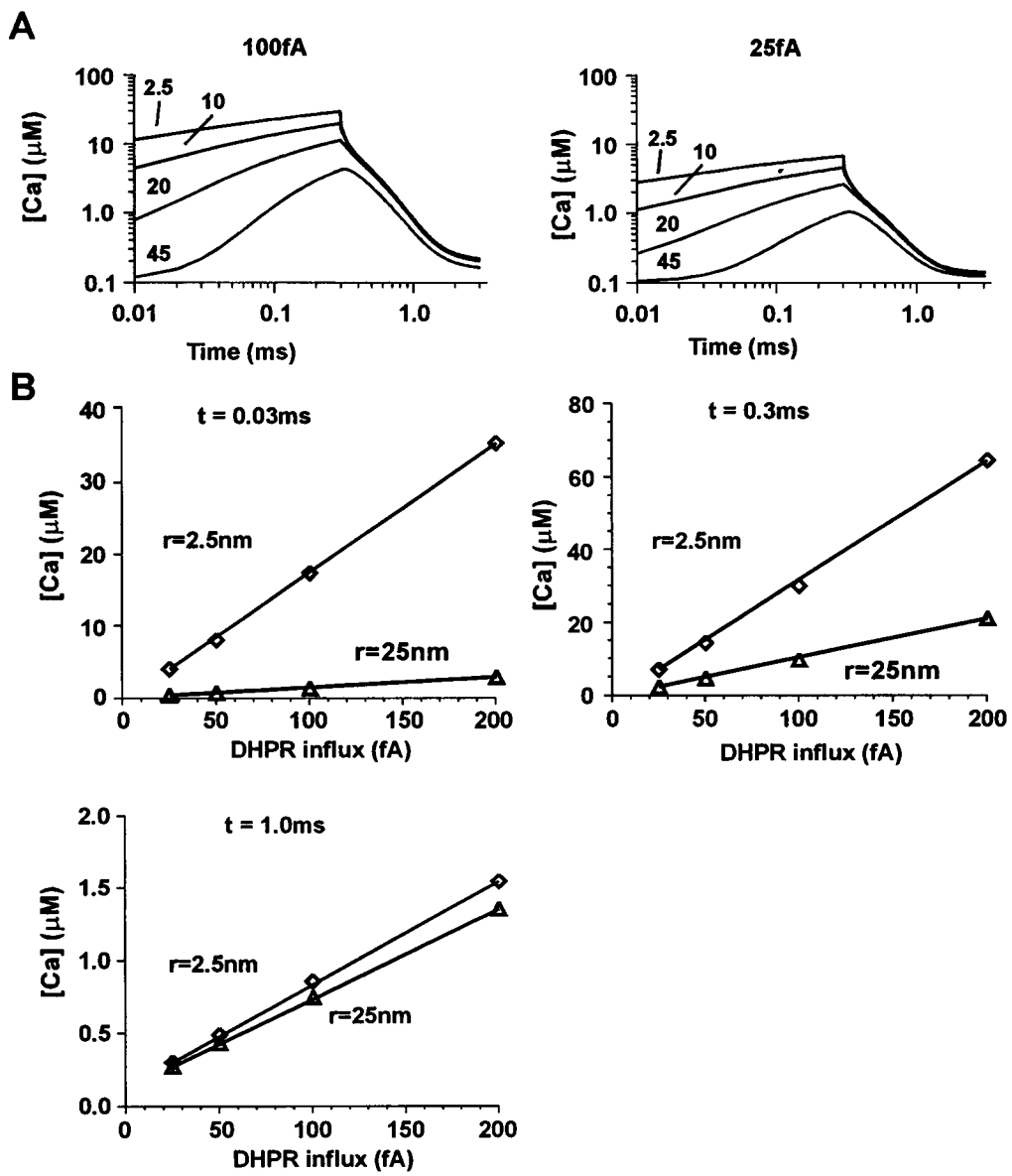


FIGURE 10 Dependence of the time course of $[Ca^{2+}]$ on DHPR channel current. (*A*) $[Ca^{2+}]$ at various radial distances and 4 nm from the SR membrane in a 100-nm diad. *Left*: The changes in $[Ca^{2+}]$ resulting from a 100-fA DHPR current lasting 0.3 ms. *Right*: $[Ca^{2+}]$ changes associated with a 25-fA DHPR current. (*B*) Summary of the temporal and radial dependence of $[Ca^{2+}]$ as DHPR current is varied. The three graphs show $[Ca^{2+}]$ levels at 2.5 and 25 nm from the center of the diad at 0.03, 0.3, and 1 ms. Note the near-linear dependence of $[Ca^{2+}]$ on DHPR current in all cases.

current, so that the buffer systems are behaving nearly linearly. This observation may prove useful in allowing extrapolation of our graphs to other single-channel currents.

## DISCUSSION

The computer model presented here has allowed investigation into the likely levels of $[Ca^{2+}]$ that will develop when DHPRs open. It is apparent that the surface charge on the inner face of the sarcolemma has a large effect on distribution of $[Ca^{2+}]$ after DHPR opening. This effect has been largely ignored in previous computations, although the effect of surface charge on the amount of calcium bound to the sarcolemma has been explored by others (Bers et al., 1985). In other numerical studies of calcium diffusion in the presence of mobile and immobile buffers, a rapid buffering approximation has been used that assumes instantaneous equilibrium of $[Ca^{2+}]$ with the relevant buffers (Langer and Peskoff, 1996; Peskoff et al., 1992). This approximation is valid only if the equilibration time of the calcium-buffer reactions is much smaller than the time required for $[Ca^{2+}]$ to diffuse the distance over which gradients exist (Smith et al., 1996); in terms of Eq. 14, $|\nabla \cdot J| \gg |F(\mathrm{Ca}, t)|$. However, as shown by the results presented here, the typical diffusion time over the width of the diad is $\ll 1$ ms, whereas buffers equilibrate over time scales on the order of $\sim 1$ ms. Therefore, the use of steady-state corrections to solve the reaction/diffusion equations for this type of system is problematic.

In the following discussion we will not consider the effects of the various geometries and binding sites in detail, as they are self-evident from the presented graphs. Instead, we will concentrate on the major effects of the electric field and phospholipid-binding sites from the viewpoint of achieving a responsive E-C coupling system.

### Effect of surface charge in the diad

We avoided difficulties associated with solving the Stokes-Einstein equation by assuming that $d\phi/dh$ is an exponential function with a constant Debye length; this assumption seems justifiable in view of 1) the presence of high concentration of monovalent ions and 2) the fact that the radius of curvature of the membranes seen in electron micrographs is much larger than the Debye length (1 nm). With these simplifications, the solution of the equations became possible on a fast workstation.

It is clear that the electric field results in marked changes in the distribution of calcium within the diad, an effect that should not be ignored when considering $[Ca^{2+}]$ changes during E-C coupling. Although a previous simulation (Peskoff et al., 1992) has calculated the amount of calcium bound to the membrane by adjusting the apparent phospholipid-binding constant on the basis of steady-state measurements (Post and Langer, 1992), the electric field effects cannot be reproduced by any steady-state corrections to the phospholipid-binding constant because the binding constant correction will be dependent on the $[Ca^{2+}]$ near the membrane, which is both potential sensitive and time dependent (Figs. 3 and 4). In addition, the accumulation of calcium near the membrane by the electric field results in the phospholipids binding calcium at a higher rate than would be predicted by diffusion-limited on rates and the average $[Ca^{2+}]$ between the SR and t-tubule membranes. Nevertheless, our calculations further reinforce the view that the phospholipid calcium-binding sites act as the major sink for calcium in the diad during E-C coupling (Peskoff et al., 1992; Langer and Peskoff, 1996).

The electric field causes calcium to accumulate near the membrane, and this reduces the $[Ca^{2+}]$ levels within the cleft. This effect is equivalent to the diadic space having a volume larger than would be expected from its geometry (an apparent volume expansion). As far as E-C coupling is concerned, this volume expansion will reduce the probability that CICR is activated and might be considered to be equivalent to an apparent increase in the distance between the SR and t-tubule membranes. However, this apparent volume expansion does not reduce the rapidity of the rise of $[Ca^{2+}]$ in the cleft in the same way that an equivalent increase in the distance between the SR and t-tubule membranes would. It should also be noted that the volume expansion does not lead to an increase in the amount of diffusible calcium-binding sites (such as calmodulin) within the diad. (Indeed, if the diffusible calcium-binding sites had a significant negative charge density, they would be electrostatically repelled from the expanded volume.) It is intriguing to consider that the volume expansion by the electric field effectively increases the ratio of free calcium to bound calcium within the diadic space in a way that may not be reproduced by any other combination of calcium-binding sites.

Because the calcium diffusion coefficient may be slower toward the edge of the diad than between the SR and t-tubule membranes (because of the tortuosity factor associated with the large RyRs), it is possible that the surface charge and electric field may augment the efficiency of E-C coupling by reducing the rate of decline of $[Ca^{2+}]$ after the DHPR closes (Fig. 4 *D*). This effect would arise from the volume expansion, providing a virtual store of calcium with very fast kinetics. Put another way, the calcium previously attracted into the electric field is released with a diffusion-limited rate constant, and this high off-rate constant cannot be mimicked by any binding site with a diffusion-limited on rate and reasonable affinity. This virtual store will therefore continue to supply calcium to any nonequilibrated calcium-binding sites within the diad for a short period after the DHPR closes. This fast calcium store is further augmented on a slower time scale by calcium release from the phospholipids (as suggested by Peskoff et al., 1992; Langer and Peskoff, 1996) to limit the rate of fall of $[Ca^{2+}]$ within the diad. It is possible that such effects may offset the reduction in $[Ca^{2+}]$ levels by the electric field by causing calcium to be elevated for a slightly longer period after channel closure and thereby maintain the efficiency of CICR activation.

In connection with this point, the model predicts that, for a given amount of sarcolemmal calcium binding, the electric field allows calcium to be released more rapidly by the sarcolemma to accelerate the decline of $[Ca^{2+}]$ at later times. Therefore the combination of the electric field with sarcolemmal calcium-binding sites may actually help increase the responsiveness of CICR. For animals needing heart rates over 100 $s^{-1}$, these effects help return $[Ca^{2+}]$ in the diad to near-resting levels between beats and may therefore confer distinct evolutionary advantages.

## Effect of diad geometry

Our calculations show that increasing the diameter of the diad leads to a decrease in the uniformity of $[Ca^{2+}]$ over the diad as well as a slowing in the time course of decline of $[Ca^{2+}]$ after DHPR closure. Although we have been unable to find any stereological measurements of diad shapes, our simulations suggest that the principal effect of increasing diad diameter will be to increase the time course of decline of $[Ca^{2+}]$. Therefore, for equal junctional areas, 16 diads 100 nm in diameter would (on average) allow tighter control of junctional $[Ca^{2+}]$ levels than a single diad 400 nm in diameter. However, further reductions in diad diameter eventually lead to a reduction in peak $[Ca^{2+}]$ levels (as a free diffusion situation is approached). SR calcium release channels are large, so it would be impossible to combine large numbers of release channels in small diads. We therefore suggest that if large numbers of tightly controlled release channels are required, it would be advantageous to have large numbers of small diads (100–200 nm) or oval-shaped diads with a small minor axis (of ~100–200 nm) and a longer major axis (>200 nm). In view of this suggestion, it is remarkable that skeletal muscle has developed a triad structure composed of very narrow but long diad type structures. Such an arrangement would certainly augment the speed of deactivation of CICR-based E-C coupling, but would also incur the penalty of lower peak $[Ca^{2+}]$ levels inside the diad (as calcium would be lost more readily from the diad center). It is therefore possible that the evolutionary need to develop an even faster form of E-C coupling in skeletal muscle forced the modification of CICR to overcome the latter disadvantage, resulting in a system in which the DHPR directly controls the RyR.

We thank I. M. Wall for his help with some preliminary calculations of $[Ca^{2+}]$ levels in the diad.

This work was supported by a grant from the Wellcome Trust (U.K.).

## REFERENCES

Bers, D. M. 1991. Excitation-Contraction Coupling and Cardiac Contractile Force. Kluwer, Dordrecht, The Netherlands.

Bers, D. M., K. D. Philipson, and A. Peskoff. 1985. Calcium at the surface of cardiac plasma membrane vesicles: cation binding, surface charge screening, and Na-Ca exchange. *J. Membr. Biol.* 85:251–261.

Cannell, M. B., and D. G. Allen. 1984. Model of calcium movements during activation in the sarcomere of frog skeletal muscle. *Biophys. J.* 45:913–925.

Cannell, M. B., J. R. Berlin, and W. J. Lederer. 1987. Effect of membrane potential changes on the calcium transient in single rat cardiac muscle cells. *Science.* 238:1419–1423.

Cannell, M. B., H. Cheng, and W. J. Lederer. 1994. Spatial non-uniformities in $[Ca^{2+}]_i$ during excitation-contraction coupling in cardiac myocytes. *Biophys. J.* 67:1942–1956.

Cannell, M. B., H. Cheng, and W. J. Lederer. 1995. The control of calcium release in heart muscle. *Science.* 268:1045–1050.

Cannell, M. B., and C. Soeller. 1997. Numerical analysis of ryanodine activation by L-type channel activity in the cardiac muscle diad. *Biophys. J.* 73:112–122.

Carafoli, E., and A. L. Lehninger. 1971. A survey of the interaction of calcium ions with mitochondria from different tissues and species. *Biochem. J.* 122:618–690.

Coronado, R., and H. Affolter. 1986. Insulation of the conduction pathway of muscle transverse tubule calcium channels from the surface charge of the bilayer phospholipid. *J. Gen. Physiol.* 87:933–953.

Crank, J. 1975. Diffusion in heterogeneous media. *In* The Mathematics of Diffusion, 2nd Ed. Clarendon Press, Oxford. 281–285.

Delahay, P. 1965. Structure of the diffuse double layer in the absence of specific absorption. *In* Double Layer and Electrode Kinetics. Interscience Publishers, New York. 33–35.

Fabiato, A. 1983. Calcium-induced release of calcium from the cardiac sarcoplasmic reticulum. *Am. J. Physiol.* 245:C1–C14.

Fawcell, D. W., and N. S. McNutt 1969. The ultrastructure of the cat myocardia. I. Ventricular papillary muscle. *J. Cell. Biol.* 42:1–45.

Forbes, M. S., and N. Sperelakis. 1982. Bridging junctional processes in coupling of skeletal, cardiac and smooth muscle. *Muscle Nerve* 5:674–681.

Forssmann, W. G., and L. Girardier. 1970. A study of the T-system in the rat heart. *J. Cell Biol.* 44:1–19.

Hille, B. 1992. Ionic Channels of Excitable Membranes, 2nd Ed. Sinauer Associates, Sunderland, MA.

Holroyde, M. J., S. P. Robertson, J. D. Johnson, R. J. Solaro, and J. D. Potter. 1980. The calcium and magnesium binding sites on cardiac troponin and their role in the regulation of myofibrillar adenosine triphosphatase. *J. Biol. Chem.* 255:11688–11693.

Hope, M. J., M. B. Bally, G. Webb, and P. R. Cullis. 1985. Production of large unilamellar vesicles by a rapid extrusion procedure. Characterization of size distribution, trapped volume and ability to maintain a membrane potential. *Biochim. Biophys. Acta.* 812:55–65.

Isenberg, G., and S. Han. 1994. Gradation of $Ca^{2+}$-induced $Ca^{2+}$ release by voltage-clamp pulse duration in potentiated guinea-pig ventricular myocytes. *J. Physiol. (Lond.).* 480:423–438.

Kushmeric, M. J., and R. J. Podolsky. 1969. Ionic mobility in muscle cells. *Science.* 166:1297–1298.

Langer, G. A., and A. Peskoff. 1996. Calcium concentration and movement in the diadic cleft space of the cardiac ventricular cell. *Biophys. J.* 70:1169–1182.

Langner, M., D. Cafiso, S. Marcelja, and S. McLaughlin. 1990. Electrostatics of phosphoinositide bilayer membranes. *Biophys. J.* 57:335–349.

Lau, A., A. McLaughlin, and S. McLaughlin. 1981. The adsorption of divalent cations to phosphatidylglycerol bilayer membranes. *Biochim. Biophys. Acta.* 645:279–292.

López-López, J. R., P. S. Shacklock, C. W. Balke, and W. G. Wier. 1994. Local stochastic release of $Ca^{2+}$ in voltage-clamped rat heart cells: visualization with confocal microscopy. *J. Physiol. (Lond.).* 480:21–29.

López-López, J. R., P. S. Shacklock, C. W. Balke, and W. G. Wier. 1995. Local calcium transients triggered by single L-type calcium channel currents in cardiac cells. *Science.* 268:1042–1045.

McLaughlin, S., N. Mulrine, T. Gresalfi, G. Vaio, and A. McLaughlin. 1981. Adsorption of divalent cations to bilayer membranes containing phosphatidylserine. *J. Gen. Physiol.* 77:445–473.

McLaughlin, S. G. A., G. Szabo, and G. Eisenman. 1971. Divalent ions and the surface potential of charged phospholipid membranes. *J. Gen. Physiol.* 58:667–687.

Page, E. 1978. Quantitative ultrastructural analysis in cardiac membrane physiology. *Am. J. Physiol.* 235:C147–C158.

Peskoff, A., and D. M. Bers. 1988. Electrodiffusion of ions approaching the mouth of a conducting membrane channel. *Biophys. J.* 53:863–875.

Peskoff, A., J. A. Post, and G. A. Langer. 1992. Sarcolemmal calcium binding sites. II. Mathematical model for diffusion of calcium released from the sarcoplasmic reticulum into the diadic space. *J. Membr. Biol.* 129:59–69.

Post, J. A., and G. A. Langer. 1992. Sarcolemmal calcium binding sites in heart. I. Molecular origin in "gas-dissected" sarcolemma. *J. Membr. Biol.* 129:49–57.

Radermacher, M., V. Rao, R. Grassucci, J. Frank, S. F. Timerman, and T. Wagenknecht. 1994. Cryo-electron microscopy and three-dimensional reconstruction of the calcium release channel/ryanodine receptor from skeletal muscle. *J. Cell Biol.* 127:411–423.

Rose, W. C., W. Balke, W. G. Wier, and E. Marban. 1992. Macroscopic and unitary properties of physiological ion flux through L-type $Ca^{2+}$ channels on guinea-pig heart cells. *J. Physiol. (Lond.).* 456:267–284.

Saito, A., M. Inui, M. Radermacher, J. Frank, and S. Fleischer. 1988. Ultrastructure of the calcium release channel of sarcoplasmic reticulum. *J. Cell Biol.* 107:211–219.

Santana, L. F., H. Cheng, A. M. Gómez, M. B. Cannell, and W. J. Lederer. 1996. Relation between the sarcolemmal $Ca^{2+}$ current and $Ca^{2+}$ sparks and local control theories for cardiac excitation-contraction coupling. *Circ. Res.* 78:166–171.

Schieren, H., S. Rudolph, M. Finkelstein, P. Coleman, and G. Weissmann. 1978. Comparison of large unilamellar vesicles prepared by a petroleum ether vaporization method with multilamellar vesicles: ESR, diffusion and entrapment analyses. *Biochim. Biophys. Acta.* 542:137–153.

Simon, S. M., and R. R. Linas. 1985. Compartmentalization of the submembrane calcium activity during calcium influx and its significance in transmitter release. *Biophys. J.* 48:485–498.

Smith, G. D., J. Wagner, and J. Keizer. 1996. Validity of the rapid buffering approximation near a point source of calcium ions. *Biophys. J.* 70:2527–2539.

Soeller, C., and M. B. Cannell. 1996. Numerical analysis of cardiac EC-coupling. *Biophys. J.* 70:A246.

Sommer, J. R., and Johnson, E. A. 1979. The ultrastructure of cardiac muscle. *In* Handbook of Physiology, Section 2, The Cardiovascular System, Vol. 1, The Heart. R. N. Berne, N. Sperelakis, and S. R. Geiger, editors. American Physiological Society, Bethesda, MD. 113–189.

Sommer, J. R., and R. A. Waugh. 1976. The ultrastructure of the mammalian cardiac cell—with special reference on the tubular membrane systems. *Am. J. Pathol.* 82:192–232.

Stern, M. D. 1992. Theory of excitation-contraction coupling in cardiac muscle. *Biophys. J.* 63:497–517.

Wang, J. H. 1953. Tracer diffusion in liquids. IV. Self-diffusion of calcium ion and chloride ion in aqueous calcium chloride solutions. *J. Am. Chem. Soc.* 75:1769–1770.